The investigation of optical and photocatalytic properties in $Dy_2M_2O_7$ (M= Hf, Zr and Ce)

halima Zaari (halimazaari@gmail.com)
Mohammed V University of Rabat: Universite Mohammed V de Rabat
khawla ouassoul
Mohammed V University of Rabat: Universite Mohammed V de Rabat
fatima zahra mezzat
Mohammed V University of Rabat: Universite Mohammed V de Rabat
fadwa el yahyaoui
Mohammed V University of Rabat: Universite Mohammed V de Rabat
abedllah kenz
Mohammed V University of Rabat: Universite Mohammed V de Rabat
benyoussef abilah
Mohammed V University of Rabat: Universite Mohammed V de Rabat

Research Article

Keywords: DFT, photocatalysis, optical properties, quantum efficiency, potential redox

Posted Date: February 22nd, 2022

DOI: https://doi.org/10.21203/rs.3.rs-1358592/v1

Abstract

A great effort has been done to improve the efficiency of materials for photo-catalytic water splitting application. The most famous catalysis is TiO_2, but its band gap, exceeds 3.0 eV, doesn't fit into the visible spectrum. so, to exploit this range of energy, we are looking for other materials having band gap lower that 2.0 eV. The research focused on the enhancement of photo-catalysis by modification of TiO_2 by means of metal loading, metal ion doping, …

This paper aims to present a group of compounds $Dy_2M_2O_7$ (with M = Hf, Ce and Zr) which could be an alternative having the same function as TiO_2.

Based on our studies and those reported in the literature, we will discuss in detail the roles and the functional mechanism of the catalysts. The results show that $Zr_2Dy_2O_7$ is the best candidate to be a photo-catalyst: it has a band gap close to 2.2 eV, and a good absorption in visible range compared to the other compound having absorption in UV. The quantum efficiency of $Zr_2Dy_2O_7$ reaches up to 3%, and the limit of conduction band and valence band are localized in potential redox zone.

Doping with Cerium gives another energy level which allows to have other optical transitions, improve the absorption and reach the quantum efficiency to 4% in a visible range.

1. Introduction

Guided by the growing energy needs, greenhouse effect and crisis of the fossil fuel resources, the search for renewable energy has become an important part of research interest [1, 2]. The hydrogen energy is widely considered as one of these potential energy vectors [3, 4]. Accordingly, the production of hydrogen using sunlight is promising approach toward economical, environmentally friendly energy [5–6–7]. Consequently, the photo-catalytic water splitting is attracting considerable interest. The photo-catalysis process is based on the activation of a semiconductor by the sunlight, thus, generates electron-hole pair and photocatalyst becomes in excited state. Afterwards, the generated electron-hole pair moves to the surface of the solid. At the interface of solid and water, transported electrons and holes reduce and oxidize the adsorbed matter.

To determine the role of crystal structure on photocatalytic activity, a variety of materials with different crystal structures need to be tested. The following material are identified as photocatalysts and active materials: $SrTiO_3$, $KTaO_3$, $NaTaO_3$ $Sr_2M_2O_7$ (M = Ta, Nb), $RbNdTa_2O_7$ and $La_2Ti_2O_7$ [8–9]

Rare earth-based materials are known for their use in the field of high and low temperature fuel cells, gas storage/separation, heterogeneous photo-catalysis, wastewater treatment, fluorescence, photo-electrochemical water. A different example of these materials could be cited like: $La_2Zr_2O_7$, known as a semiconductor, has a band gap of 3.82 eV [10], its optical and electronic properties are modified using Ce doping at Zr site, new transitions appeared in the absorption spectra for 3.4% Ce doped $La_2Zr_2O_7$.[11].

The modified system shows an interesting behavior in the thermal conductivity, which increases as a function of temperature compared to the pure $La_2Zr_2O_7$. In addition, the effect of each concentration of Ce is studied and shows that 3.4% of Ce provides the lowest thermal conductivity, the last one attributed to the high concentration of point defects affecting the phonon scattering. [11]

Experimental and theoretical study of $Sm_2Zr_2O_7$ and $Dy_2Zr_2O_7$ has been done [12] to show the effect of Dy doped $Sm_2Zr_2O_7$ on the band gap and ionic conductivity, the system has a tunable band gap as function of Dy content, then its potential is explored as photo-catalyst.

The synthesis by a different procedure of $Dy_2Ce_2O_7$ and $Dy_2Zr_2O_7$ reported in [13–16] show a good thermal stability during this process and it arrived at a pure phase of $Dy_2Ce_2O_7$ at 1500°C.

In the present study, we chose $Dy_2M_2O_7$ (M = Zr, Hf, Ce) systems as photo-catalysts for water splitting and we discuss the relationship between the photocatalytic activities and the electronic properties (band gap). using ab-initio calculations, geometrical structure, electronic band structure and optical properties of pure $Dy_2M_2O_7$ will be calculated for (M = Hf, Ce, Zr).

There are a few details for $Dy_2Hf_2O_7$, so we aim to study all of the three systems and look for points of difference and resemblance of them based on the comparison of the electronic and optical properties.

Our study is based on DFT calculation, in its Kohn-Sham (KS) formulation, where exchange-correlation effect has been approximated, then the results depend on the chosen of approximation (LDA, GGA) [17–18]. The problem appears when we get an underestimation of the KS band gap compared to the experimental ones. In fact, the KS band gap is the difference in the eigenvalues of the conduction-band minimum and the valence-band maximum, the experimental band-gap is the difference between the ionization potential and the electron affinity [19]. To solve this problem many approximations have been proposed, such as GGA + U and the modified Becke-Johnson potential (mBJ) [20–21]. The contribution of these approximations was well discussed, and it was noted that the correction depends on the nature of material, however in generally, the mBJ correction reproduces a good value in band gap. For this reason, we have used GGA + mBJ potential including spin-orbit coupling in our calculation. In addition, GGA + U localized the f and d states by applying the right value of U, in our case we estimated to have the exact values for the valence band limit and the conduction band limit which further justifies our choice of mBJ approach. These values will be used to confirm the photo catalytic application of our materials.

2. Computational Details

In order to describe the electronic and optical properties of pure $Dy_2M_2O_7$ (M = Hf, Ce and Zr), we used the full potential linearized augmented plane wave (FP-LAPW) method implemented in the WIEN2K code [22], within the framework of density functional theory (DFT), by treating the exchange and correlation in the level of the GGA-Perdew-Burke-Ernzerhof (GGA-PBE) approximation [23].

The basic functions, the electron densities and the potential were investigated in self-consistent manner. These quantities are developed by dividing the unit cell into non-overlapping atomic spheres, where a linear combination of radial functions times spherical harmonics is used with a cut-off parameter l_{max} =10. Moreover, an interstitial region where a plane wave expansion is used with a cut-off parameter RMT*K_{max} = 9, (RMT is the smallest muffin-tin radius in the unit cell and K_{max} is the magnitude of the largest K wave vector).

The muffin-tin sphere radii used in the calculations are (2.37, 2.08, 1.88, a.u) for Dy, Zr, O respectively,

(2.35, 2.09, 1.8) for Dy, Hf and O respectively, and (2.25, 2.32, 1.84) for Dy, Ce and O respectively.

The results are obtained with an energy convergence criterion of 10^{-4} Ry. We used a (10*10*3) grid with 50 special points for sampling [24], corresponding to 400 k-points in the irreducible Brillouin zone for $Dy_2Ce_2O_7$, and (7*7*7) grid with 172 special points corresponding for both $Dy_2Hf_2O_7$ and $Dy_2Zr_2O_7$.

The spin-orbit effect is also taken into calculation and TB-mBJ potential to correct the band gap value.

- The valence and conduction band edge were computing by the following equation:

$E_{CB}^{0} = \chi(S) - E^{0} - \frac{1}{2}E_{g}$(1),

$$E_{VB}^{0} = E_{CB}^{0} + E_{g}$$

2

Where χ(S) is the Mulliken electronegativity and E_g is the band gap energy E^0 is the scale factor relating the electrode redox level to the absolute vacuum scale (AVS) ($E^0 \sim 4.5$ eV for normal hydrogen electrode (NHE)). [25]

- Effective mass of electrons and hole for the three compounds is computed using the fit of the equation [26]:

$$E(k) = E_0 + \frac{\hbar^2 k^2}{2m*}$$

3

Where $E(\mathbf{k})$ is the energy of an electron at wavevector **k** in that band, E_0 is a constant giving the edge of energy of that band, and m^* is a constant (the effective mass).

We can make a fit of the band in the direction Γ and M with the parabolic equation (for 8 points) mentioned before; we derive twice to calculate the effective mass for the holes and the electrons.

3. Result And Discussion

3.1 Electronic and Optical properties:

$Zr_2Dy_2O_7$ and $Dy_2Hf_2O_7$ are crystalized in a fluorite structure (Fm3m), $Dy_2Ce_2O_7$ crystallized in an orthorhombic structure (Pmma) as shown in Table 1.and Fig. 1.

With these structures, the nature of the atomic radius of each atom, the degree of oxidation one can predict magnetically and the electronic behavior of these compounds are shown in Table 2. However, a deep study on the behavior of each material will be made subsequently based on the theoretical simulation.

Table 1
Structural properties $Dy_2Ce_2O_7$, $Dy_2Zr_2O_7$, $Dy_2Hf_2O_7$

	$Dy_2Hf_2O_7$	**$Dy_2Zr_2O_7$**	**$Dy_2Ce_2O_7$**
Lattice parameter (A)	10.5[28]	5.23 [29]	a = 3.37 ; c = 10.9 [31]
Optimized value	10.48	5.24	**a = 3.38, c = 10.7**

Table 2
electronic configuration and valence states of Dy, Zr, Ce and Hf atoms.

	Dy	**Zr**	**Ce**	**Hf**
Electronic Configuration	$4f^{10}\ 6s^2$	$4d^2\ 5s^2$	$4f^1\ 5d^1\ 6s^2$	$4f^{14}\ 5d^2\ 6s^2$
Oxidation	3	4	3,**4**	4
Valence	$4f^9$	$4d^0$	$4f^0$	$4f^{14}\ 5d^0$

Based on the Table 2; the degree of oxidation allows us to know the occupied states, the empty states and to predict possible allowed optical transitions.

to ensure the neutrality in $Dy_2Ce_2O_7$ oxidation degrees are: Ce^{4+} Dy^{3+} O^{2-}, thus all the f-Ce states, d and s states are localized in conduction band, however the f-Dy states are those which will mainly contribute to valence band for the 3 types of compounds.

Based on the Figs. 2, 3,4 and Table 2; the valence band is constituted by p-O and f-Dy states, other states are localized on the conduction band. Therefore, all the allowed optical transitions are p-d and f-d: p-orbital of oxygen to d-orbital of Zr and Hf.

$Dy_2Hf_2O_7$, $Dy_2Zr_2O_7$ and $Dy_2Ce_2O_7$ **have an electronic band gap close** to 1.89, 2.0 and 1.4 eV respectively.as cited in Table 3 compared to other works. These values are obtained using GGA and mBJ potential including spin-orbit coupling. It is well known that standard LDA and GGA are not appropriate to compute the band gap since giving too small band gaps or even a wrong metallic behavior rather than an insulating one in some cases.

Table 3
Band gap of the 3 compounds compared to other works.

	$Dy_2Hf_2O_7$	$Dy_2Zr_2O_7$	$Dy_2Ce_2O_7$
Band gap (eV)	2.946 eV [28]	3.18 [30]	2.75 exp [31]
Our results	1.89 eV	2.0	**1.4**

The band structure of the 3 compounds is illustrated on the Figs. 5 and 6, we have a direct band gap for the 3 types, with different values, the spin-orbit effect is already considered in the calculation and mBJ potential. These figures will be exploited to interpret the variation in effective mass qualitatively and quantitatively using the Eq. (3).

In fact, the decisive factor for the effective mass is the curvature of the dispersion curve at the top level, as in the second derivative. Large curvatures (large second derivative = small radius of curvature) give small values of the effective mass. On the other hand, small curvatures (small derivative of a second = large radius of curvature) give large values of the effective mass.

Table 4 gives the values of effective mass in Γ and M direction, we can see that these values are important in M and Γ direction for down states, for both electrons and holes, the opposite for the up states in the same directions, the values of m* are very low.

The mobility of charge carriers in a semiconductor is inversely proportional to their effective mass (m*). Thus, $Dy_2Hf_2O_7$ and $Dy_2Zr_2O_7$ have high mobility compared to $Dy_2Ce_2O_7$.

According to these values of effective mass, we can deduce the lifetimes of the photo-excites charge carriers and controlling the quantum efficiency of the photo-to-current conversion mechanism in photo-catalysis process [32]

Table 4: Effective mass values for Dy_2 (Ce, Hf, Zr)O_7

$Dy_2Hf_2O_7$	Γ direction Up	Dn	M Up	dn
holes $*m_0$	-0.038	-0.43	-0.049	-13.97
electrons (m/m_0)	0.039	10.55	0,0054	infini

$Dy_2Ce_2O_7$	Γ direction		M	
	Up	down	Up	dn
holes $*m_0$	-0.92	-0.479	-0.057	-0.18
electrons (m/m_0)	0.07	0.27	0.057	0.238

$Dy_2Zr_2O_7$	Γ direction		M	
	Up	Dn	Up	dn
holes $*m_0$	-0.032	-0.11	-0.043	-84.74
electrons (m/m_0)	0.046	0.22	0.063	0.18

3.2 Optical properties and Quantum efficiency

A photocatalytic application requires a good absorption in the visible spectrum and a good optical performance, to confirm that the materials $Dy_2M_2O_7$ can be photocatalytic, we calculated the optical properties of these materials precisely: absorption coefficient and quantum efficiency.

The quantum efficiency *QE* is an important parameter for its proportionality to the quantity of electrons/holes generated by semiconductors. It is computed using the following relation [33]:

$QE=(1-R)(1-e^{-\alpha t})$ (Eq. 4)

α is the absorption coefficient α(E) and R is the reflectivity R(E). The t parameter is the thickness of the sample. Here we have used the c parameter.

According to the above relation, we have computed the absorption coefficient and quantum efficiency of all compounds; the results are displayed in Figs. 7 and 8.

There is no absorption between 0 and 2 eV in Fig. 7, except for $Dy_2Zr_2O_7$, it appears at 0.5 eV but its intensity is very weak. The first peak for $Dy_2Ce_2O_7$ appears at 1.7 eV.

In Fig. 8, we report the quantum efficiency of the 3 compound $Dy_2(Zr/Ce/Hf)O_7$; as we can see the quantum efficiency of $Dy_2Ce_2O_7$ reaches a maximum of 3% in visible range and it is very weak between 0 and 1.5 eV, both compounds have lower than 1% in the visible range.

3.3 Ce Doping effect in $Dy_2Zr_2O_7$ on the optical and electronic properties

In the last paragraph we have studied the electronic properties of Dy_2 (Hf, Ce, Zr)O_7. Now, the question is, what will happen if we doped those materials and added a new state?

To get an answer for this question, we have doped Ce atoms in $Dy_2Zr_2O_7$ (25% of Ce content) in two sites:

- The first one where Ce atoms take Zr atoms' (noted CeZr) place
- The second one where Ce atoms take Dy atoms'(noted Ce-Dy) place

We have displayed the absorption coefficient and quantum efficiency in Figs. 8 and 9.

The major difference between both cases is the Ce doped in Zr site gives large absorption from zero and the quantum efficiency varies from 2–4% in visible range.

To explain this, we look for the answer from the density of states as displayed in Figs. 10 and 11 and band structure (Figs. 12 and 13).

In Zr site; f states of Cerium, are empty (Ce^{4+} :$4f^{0}$) localized in band conduction at 3 eV above 4f-Dy states, the gap is about 1.7 eV, and the Fermi level is near the valence band (semi-conductor p type).

In Dy site, to ensure the neutrality of the system, we have (Dy^{3+} Ce^{3+} Zr^{4+} O^{-2}). Ce has the configuration: $4f^{1}$ one electron remains in valence band and it is localized near the Fermi level as shown in Fig. 13 and Fig. 14, which gives metallic behavior on the system.

3.4-Photocatalytic activity

Figure 15 presents the edges of the conduction and valence bands calculated based on absolute electronegativity, which are calculated from the ionization energy and electron affinity, and the potential H^{+}/H_2O and O_2/H_2O.

- For $Dy_2Ce_2O_7$ and $Dy_2Hf_2O_{7,}$ the gap is large and exceeds the optimal value. Even the location of the bands is out of zone.
- $DyZr_2O_7$ is the best candidate to be a catalyst because the band edges are positioned in the "redox potential" zone.
- Doping $Dy_2Zr_2O_7$ with Cerium in Zr site makes the system more accurate and promoter for photocatalytic application

4. Conclusion

To sum-up, we have used Full Potential Linearized Augmented Plan Waves to study the electronic, optical properties, quantum efficiency and photocatalytic activity for 3 different compounds ($Dy_2M_2O_7$) (M = Zr, Ce, and Hf).

This present work allows the analysis of compounds that can integrate with the family of photo catalysts through the study of 3 compounds. Through the analysis of the results obtained, it turns out that $Dy_2Zr_2O_7$ is a promising compound in photo-catalysis because of its 2.2 eV band gap. Ce doped $Dy_2Zr_2O_7$ is also a good candidate for this application.

The modification of photo-catalysts by adjusting their band structures and increasing the probability of separation of photo-generated charges to lead to the progressive development of high efficiency photo-catalysts driven by visible light. To promote the efficiency of these compounds in photo-catalysis, such

solutions are needed: Doping or co-doping with transition metal or non-metal elements or by the realization of hetero-structures or alloy structures.

We can also think of other solutions, either a modification of the structures for gap engineers or to put the band limits on the scale of the redox potential.

Declarations

Acknowledgements:

We thank P.Blaha and K.Schwarzfor the Wien2K code and the wien2k users for very useful information in the discussions.

References

1. Pérez-Lombard, L., Ortiz, J., Pout, C.: A review on buildings energy consumption information. Energy and Buildings. **40**, 394–398 (2008)
2. Dresselhaus, M.S., Thomas, I.L.: Alternative energy technologies. Nature. **414**, 332–337 (2001)
3. Elam, C.: Realizing the hydrogen future: the International Energy Agencys efforts to advance hydrogen energy technologies. Int. J. Hydrog. Energy **28**, 601–607 (2003)
4. MOMIRLAN, M., VEZIROGLU, T.: The properties of hydrogen as fuel tomorrow in sustainable energy system for a cleaner planet. Int. J. Hydrog. Energy **30**, 795–802 (2005)
5. Byrne, C., Subramanian, G., Pillai, S.C.: Recent advances in photocatalysis for environmental applications. J. Environ. Chem. Eng. **6**, 3531–3555 (2018)
6. Ahmad, H., Kamarudin, S.K., Minggu, L.J., Kassim, M.: Hydrogen from photo-catalytic water splitting process: A review. Renew. Sustainable Energy Reviews **43**, 599–610 (2015)
7. Maeda, K., Domen, K.: Photocatalytic Water Splitting: Recent Progress and Future Challenges. J. Phys. Chem. Lett. **1**, 2655–2661 (2010)
8. Selected perovskite oxides: Characterization, preparation and photocatalytic properties—A review Ewelina Grabowska Applied Catalysis B: Environmental Volume 186, 5 June 2016, Pages 97–126
9. Photocatalytic Activity of R3MO7: and R2Ti2O7 (R = Y, Gd, La; M = Nb, Ta) for Water Splitting into H2 and O2 Ryu Abe, Masanobu Higashi Kazuhiro Sayama Yoshimoto Abe Hideki Sugihara. J. Phys. Chem. B **110**, 2219–2226 (2006)
10. Effects of the: counter-cation nature and preparation method on the structure of $La_2Zr_2O_7$. William Duarte, Ariane Meguekam, Maggy Colas, Michel Vardelle. Sylvie Rossignol J Mater Sci **50**, 463–475 (2015)
11. Theoretical investigations of electronic: and thermodynamic properties of Ce doped $La_2Zr_2O_7$ pyrochlore Sahar Ramin Gul, Matiullah Khan Yi Zeng Bo Wu, Materials Research Express, Volume 6, Number 8

12. Sm2 – xDyxZr2O7 Pyrochlores: Probing Order – Disorder Dynamics and Multifunctionality Farheen, N., Sayed, V., Grover, K., Bhattacharyya, D., Jain, A., Arya, C.G.S., Pillai, Tyagi, A.K.: Inorganic Chemistry **2011** *50* (6), 2354–2365
13. Zinatloo-Ajabshir, S., Salehi, Z., Salavati-Niasari, M.: Green synthesis and characterization of Dy2Ce2O7 ceramic nanostructures with good photocatalytic properties under visible light for removal of organic dyes in water. J. Clean. Prod. **192**, 678–687 (2018)
14. Photocatalytic Activity of R3MO7: and R2Ti2O7 (R = Y, Gd, La; M = Nb, Ta) for Water Splitting into H2 and O2 Ryu Abe, Masanobu Higashi Kazuhiro Sayama Yoshimoto Abe Hideki Sugihara. J. Phys. Chem. B **110**, 2219–2226 (2006)
15. Effects of the: counter-cation nature and preparation method on the structure of $La_2Zr_2O_7$. William Duarte, Ariane Meguekam, Maggy Colas, Michel Vardelle. Sylvie Rossignol J Mater Sci **50**, 463–475 (2015)
16. Maki, Y., Matsuda, M., Kudo, T., SOLID ELECTROLYTE FUEL CELL, 1971: U.S.patent.31.Sachdeva, Chavan, A., Goswami, S.V., Tyagi, A., A.K., and Pujari, P.K. Positron annihilation spectroscopic studies on Nd-doped ceria.J. Solid State Chem., 2005. 178(6): p. 2062–2066
17. Hohenberg, P., Kohn, W.: Inhomogeneous Electron. Gas Phys. Rev. **136**, 864 (1964)
18. Kohn, W., Sham, L.J.: Self-Consistent Equations Including Exchange and Correlation Effects Phys: Rev. **140**, A1133 (1965)
19. Perdew, J.P., Parr, R.G., Levy, M., Balduz, J.L. Jr.: Density-Functional Theory for Fractional Particle Number: Derivative Discontinuities of the Energy. Phys. Rev. Lett. **49**, 1691 (1982)
20. Tran, F.: P. Blaha Accurate Band Gaps of Semiconductors and Insulators with a Semilocal Exchange-Correlation Potential. Phys. Rev. Lett. **102**, 226401 (2009)
21. Zaari, H., Hachimi, E., Benyoussef, A.G., A., & Kenz, E., A: Comparative study between TB-mBJ and GGA + U on magnetic and optical properties of CdFe2O4. J. Magn. Magn. Mater. **393**, 183–187 (2015)
22. Blaha, P., Schwarz, K., Madsen, G., Kvasnicka, D., Luitz, J.: WIEN2k, augmented plane wave local orbitals program for calculating crystal properties, Vienna, Austria. (2001)
23. Perdew, J.P., Burke, K., Ernzerhof, M.: Generalized Gradient Approximation Made Simple Phys. Rev. Lett. **77**, 3865–3868 (1996)
24. Monkhorst, J., Pack, J.: Special points for Brillouin-zone integrations. Phys. Rev. B **13**, 5188 (1976)
25. Mousavi, M., Habibi-Yangjeh, A., Abitorabi, M.: Fabrication of novel magnetically separable nanocomposites using graphitic carbon nitride, silver phosphate and silver chloride and their applications in photocatalytic removal of different pollutants using visible-light irradiation. J. Colloid Interface Sci. **480**, 218–231 (2016)
26. Green, M.A.: *(*1990*). "Intrinsic concentration, effective densities of states, and effective mass in silicon". Journal of Applied Physics.* <bi>67</bi> *(6): 2944–2954.*]
27. Kokalj, A., J. Mol. Graphics Modelling, 1999, 17, 176–179

28. Zu, X.T., Li, N., Gao, F.: First-principles study of structural and energetic properties of A2Hf2O7 (A = Dy, Ho, Er) compounds. J. Appl. Phys. **104**(4), 043517 (2008). doi:10.1063/1.2969662
29. Tong, Y., Yu, Z., Lu, L., Yang, X., Wang, X., Rapid preparation and characterization of Dy2Zr2O7 nanocrystals, Mater. Res. Bull., 43, 10, 2008, 2736–2741
30. 30.: Absence of spin-ice state in the disordered fluorite Dy2Zr2O7 JRamon, G.A., Wang, C.W., Ishida, L., Bernardo, P.L., Leite, M.M., Vichi, F.M., Gardner, J.S. and R. S. Freitas Phys. Rev. B 99, 214442 – Published 27 June 2019
31. The joint automated repository for various integrated simulations (JARVIS) for data-driven materials design, npj Computational Materials 6, 173 (2020)
32. Sangita Dutta Tilak Das, Datta, S. Phys. Chem. Chem. Phys., 2018,20, 103–111
33. Baaalla, N., Ammari, Y., Hlil, E.K.E., Kenz, A., Benyoussef: AStudy of optical, electrical and photovoltaic properties of CH3NH3PbI3 perovskite: ab initio calculations. Phys. Scr. **95**, 095104 (2020)

Figures

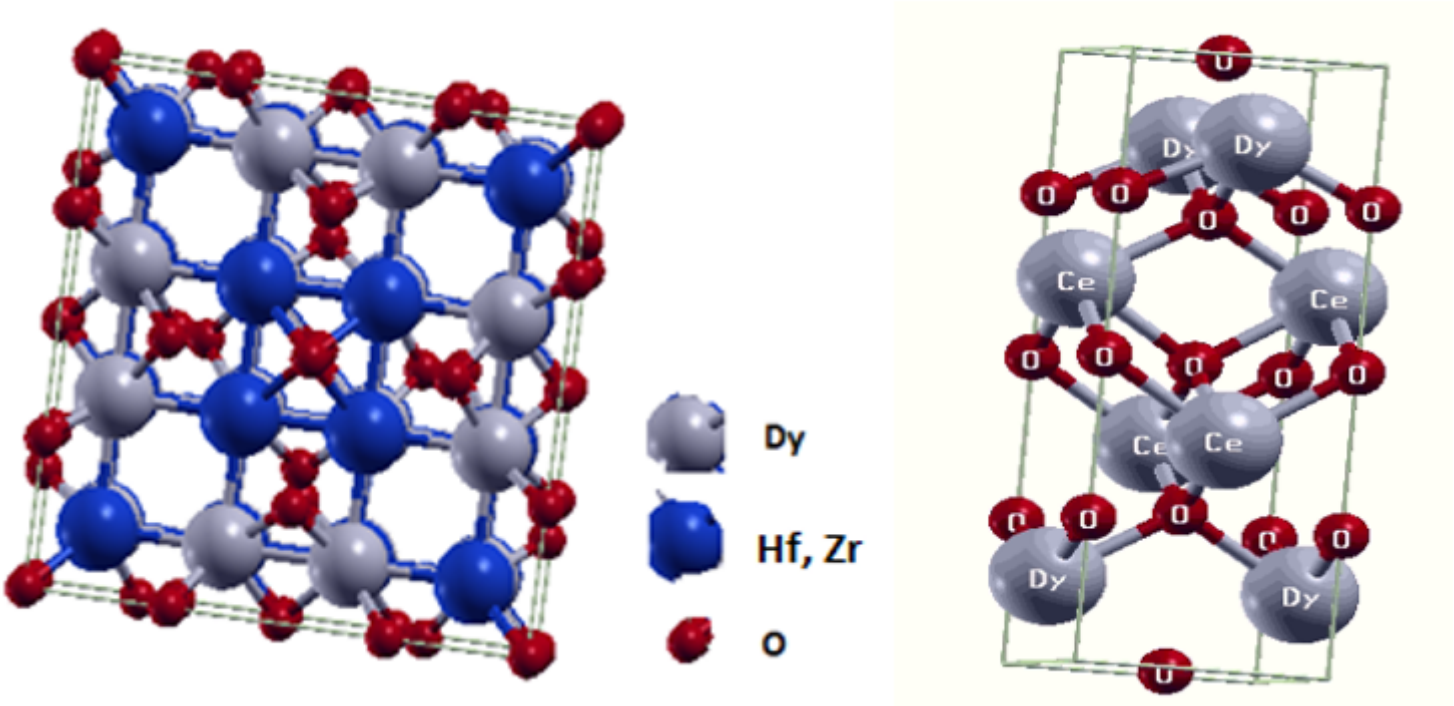

Figure 1

crystal structure of $Dy_2M_2O_7$ (M=Ce, Hf and Zr) using Xcrysden code [27]

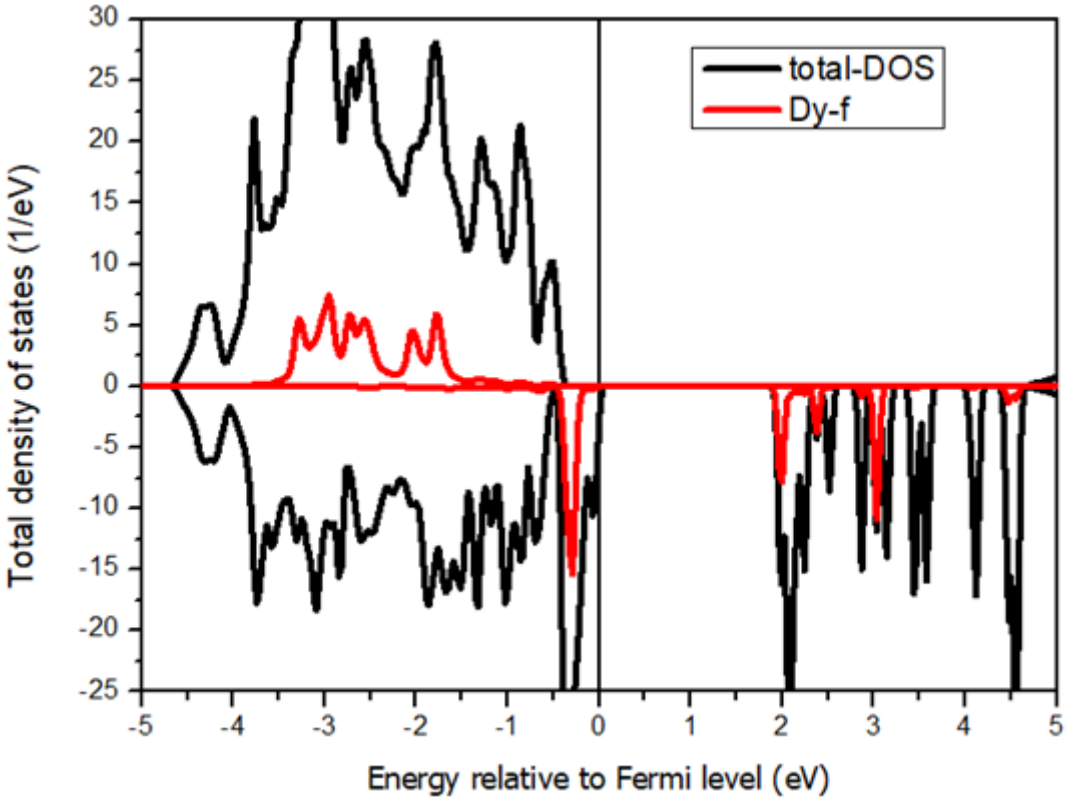

Figure 2

Total and partial density of states of $Dy_2Zr_2O_7$

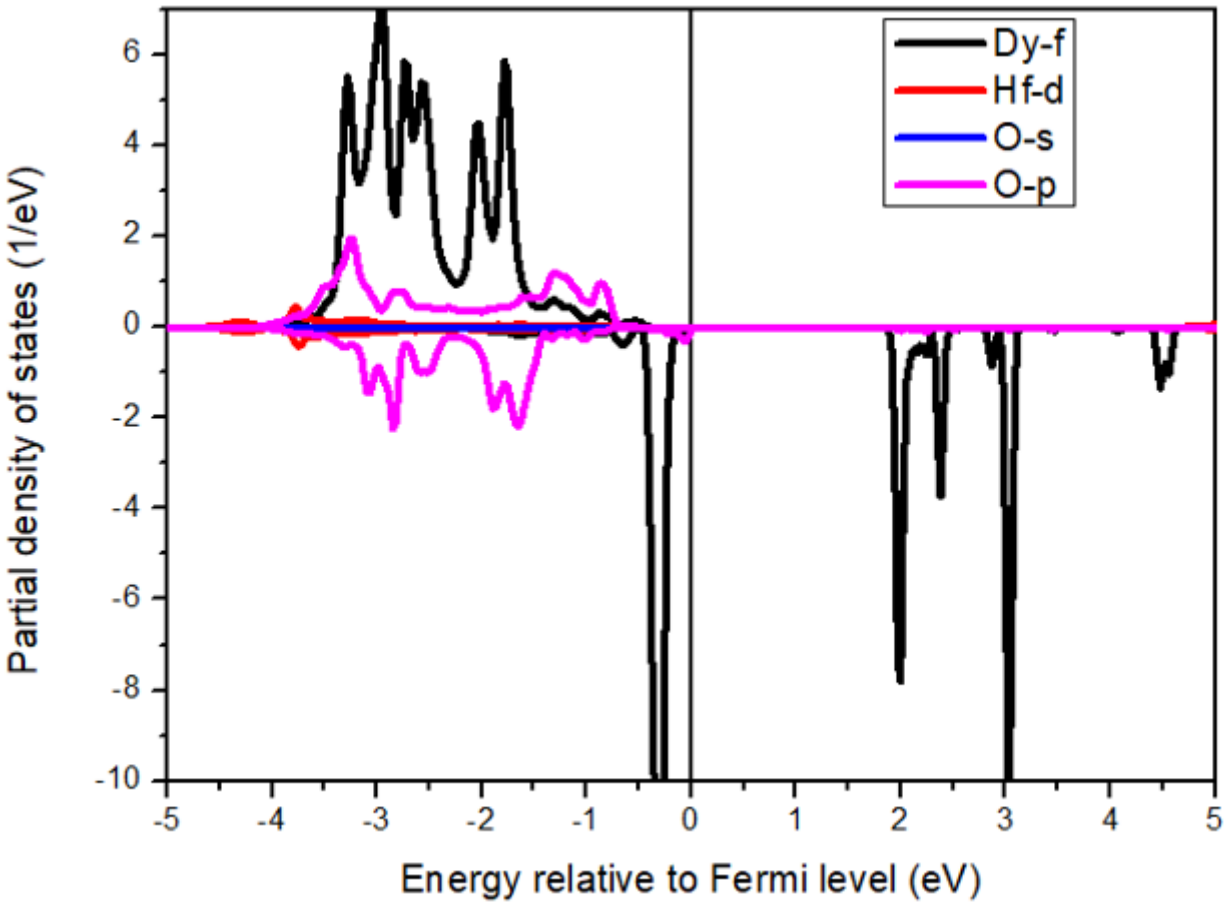

Figure 3

Partial density of states for $Dy_2Hf_2O_7$

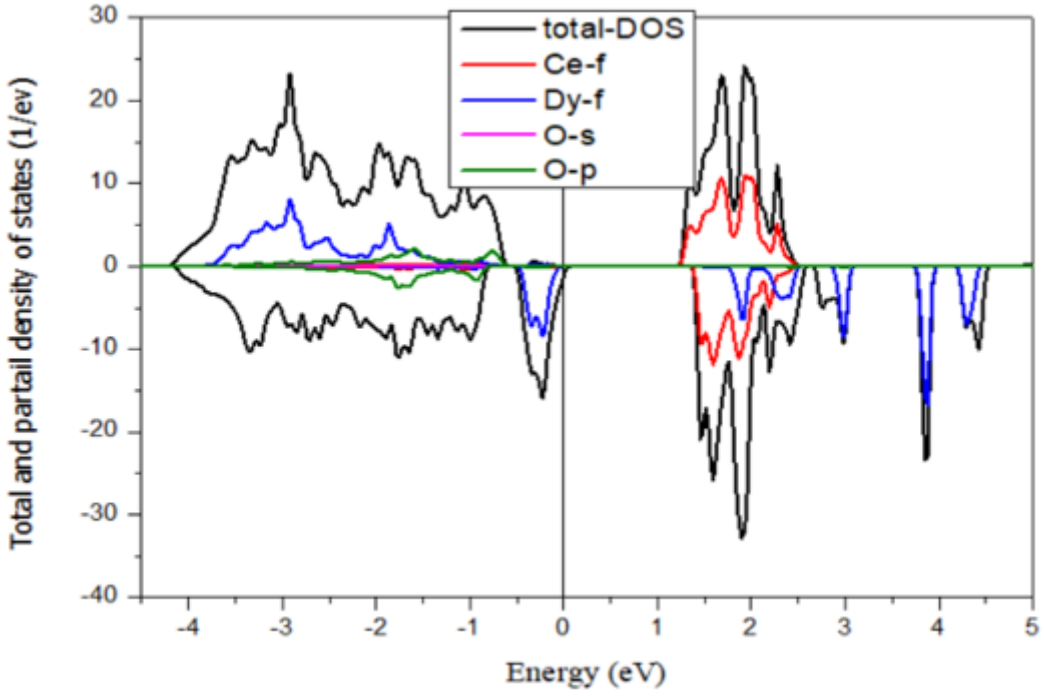

Figure 4

The total and partial density of states of $Dy_2Ce_2O_7$

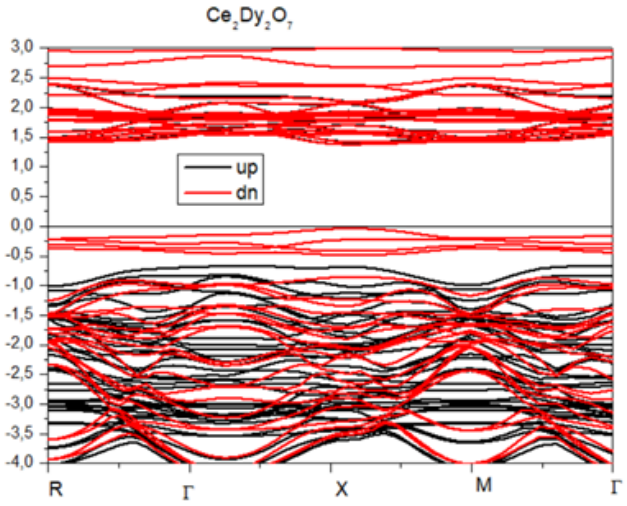

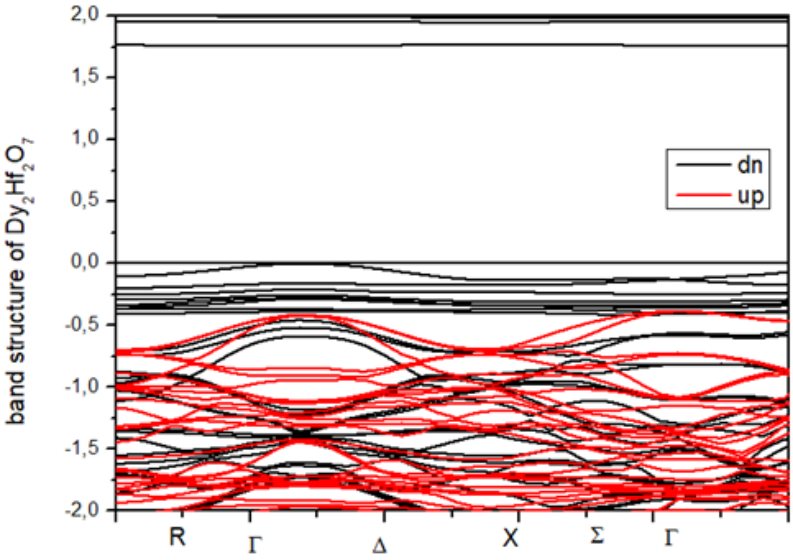

Figure 5

Band structure using mBJ approach of $Dy_2(Ce/Hf)_2O_7$ red (black) color present the states of electrons up (dn)

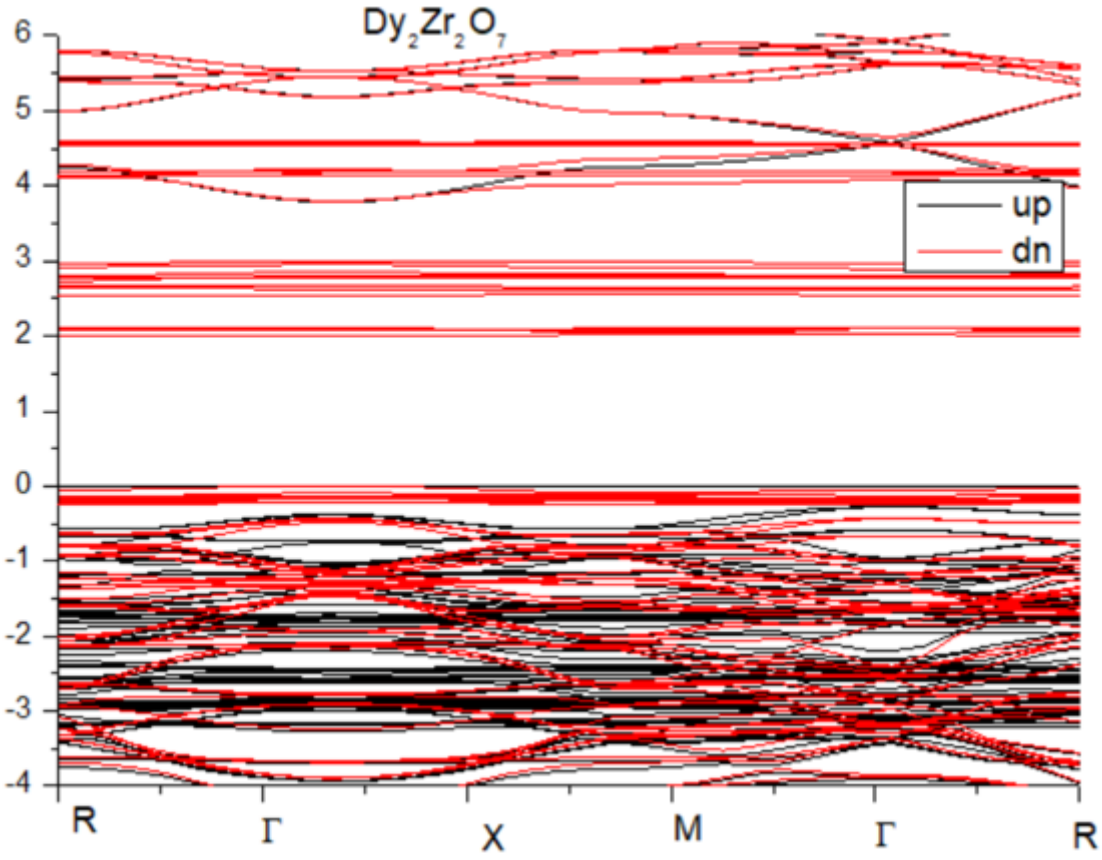

Figure 6

band structure using mBJ approach of $Dy_2Zr_2O_7$ (red=dn (black=up)

Figure 7

coefficient of absorption of $Dy_2M_2O_7$

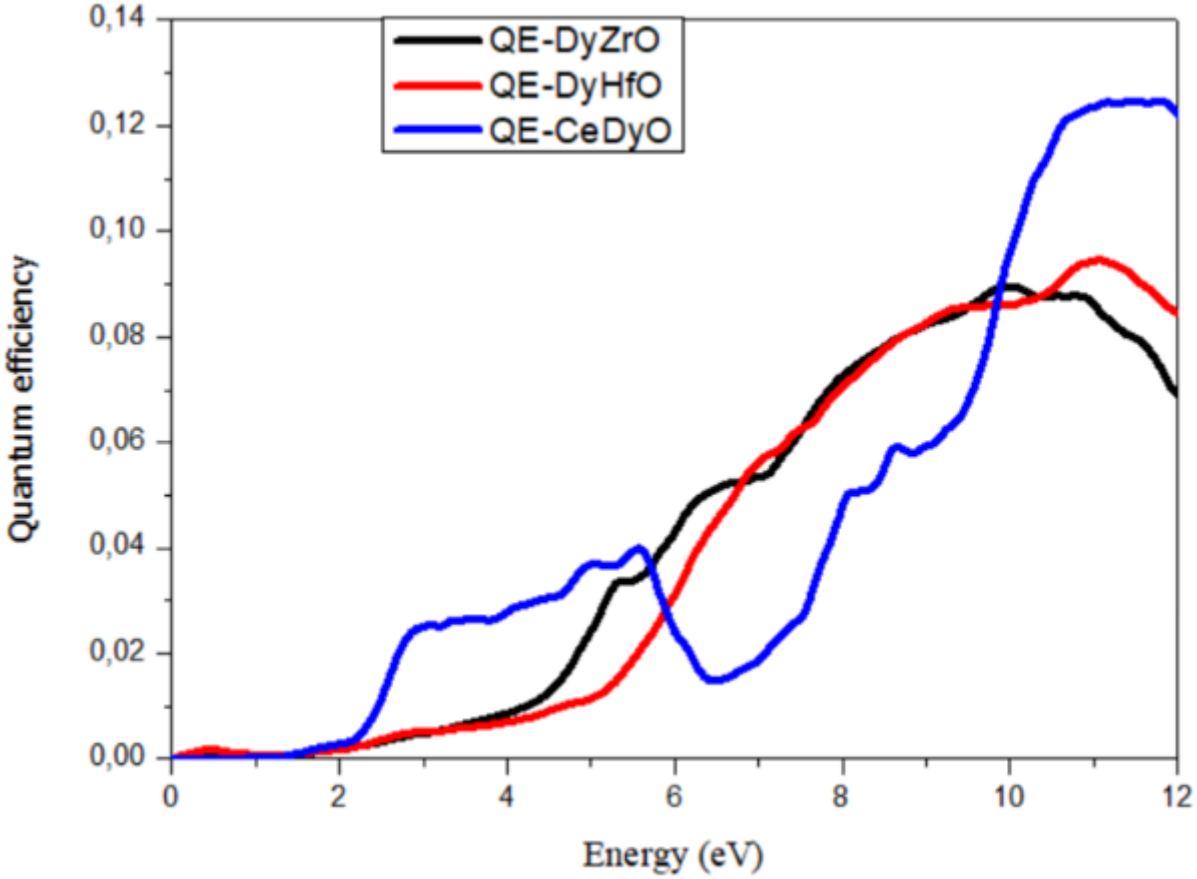

Figure 8

Quantum efficiency as function of Energy

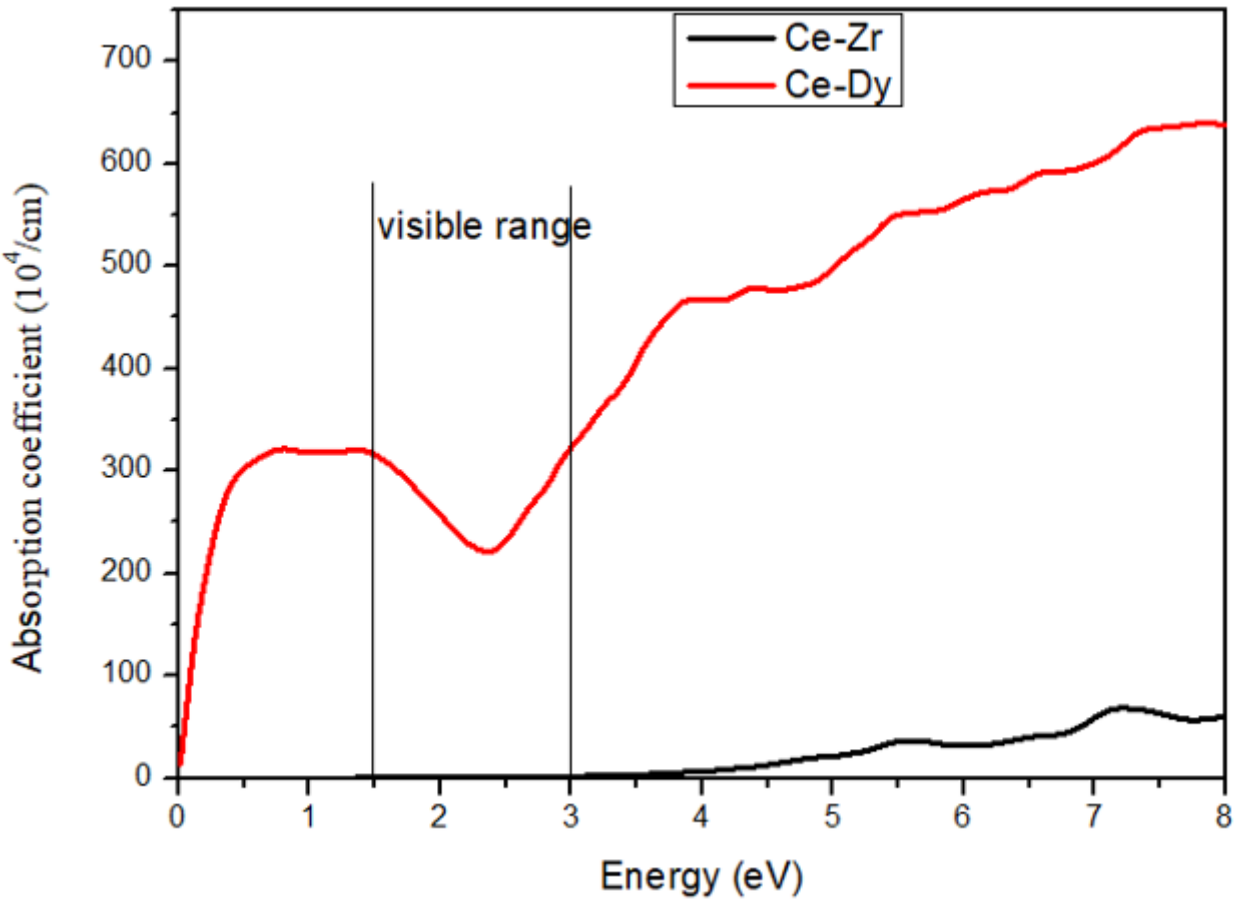

Figure 9

Absorption coefficient of Ce doped $Dy_2Zr_2O_7$

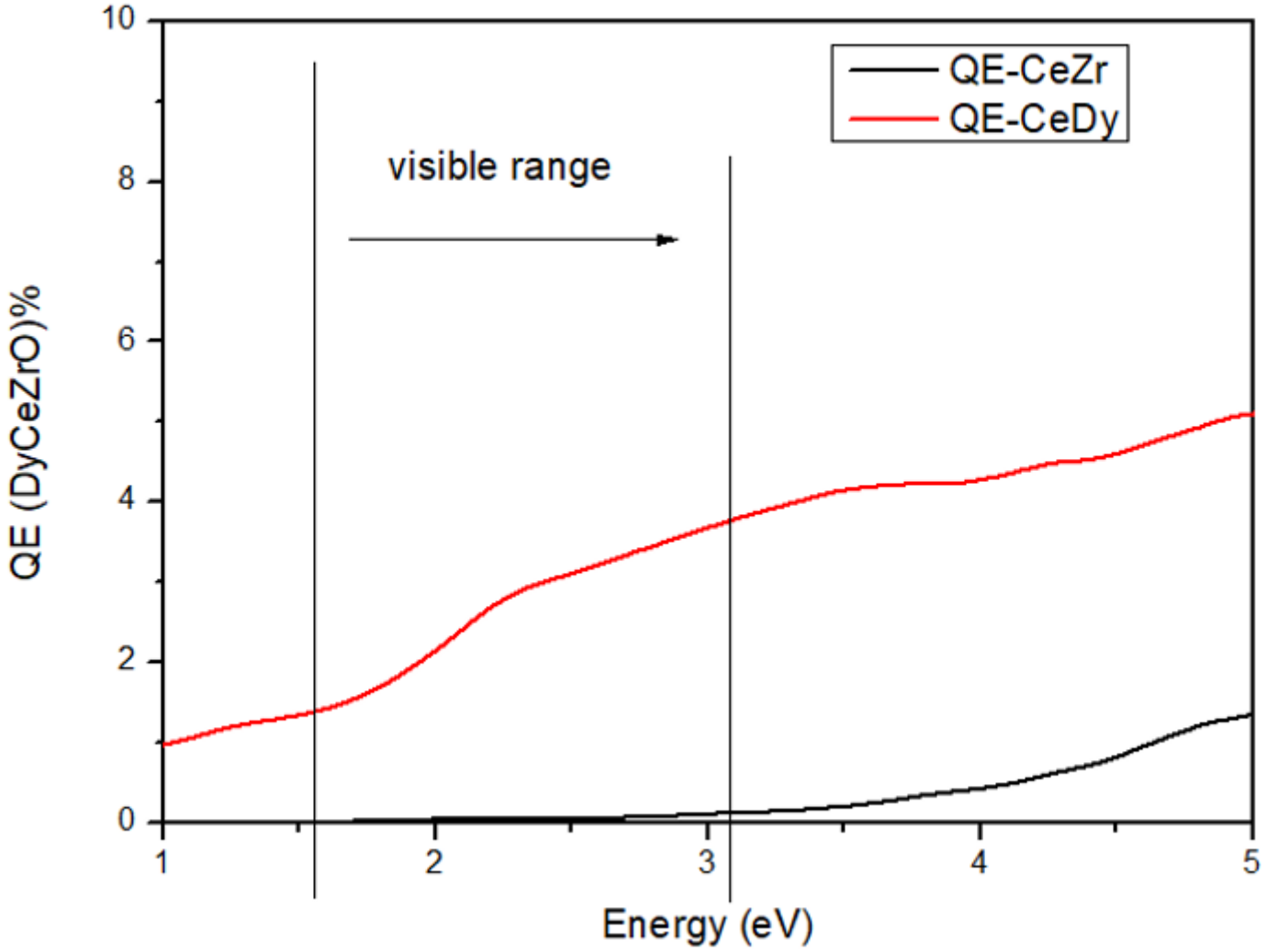

Figure 10

Quantum efficiency of Ce doped $Dy_2Zr_2O_7$

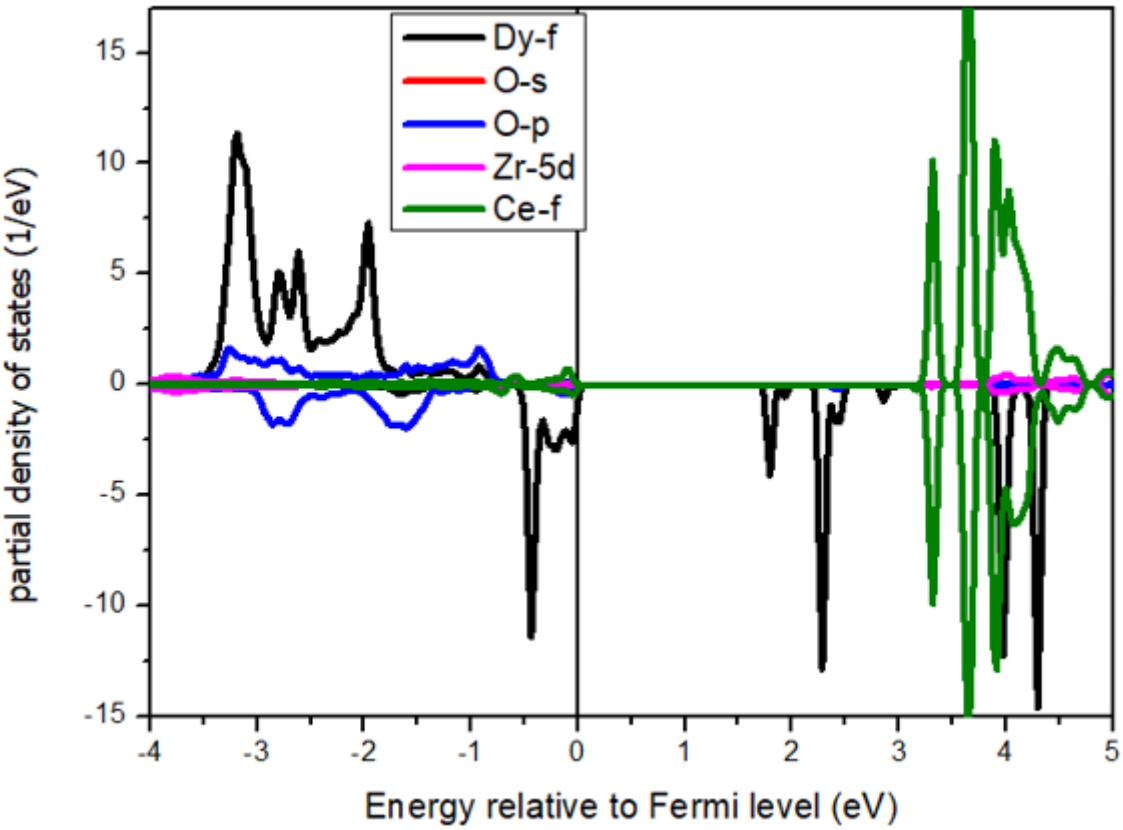

Figure 11

Partial density of states of $Dy_2(Ce_XZr_{1-x})_2O_7$

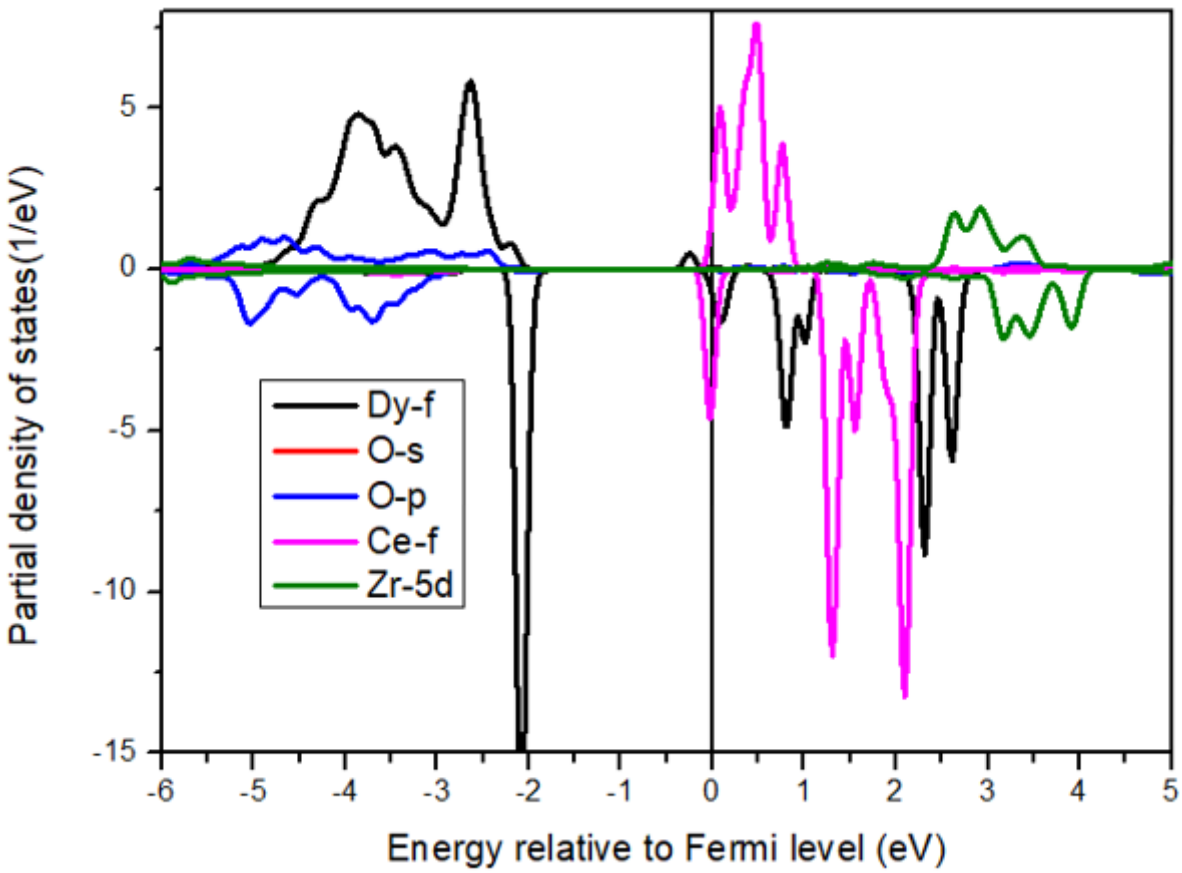

Figure 12

Partial density of states of $(Dy_{1-x}Ce_X)_2Zr_2O_7$

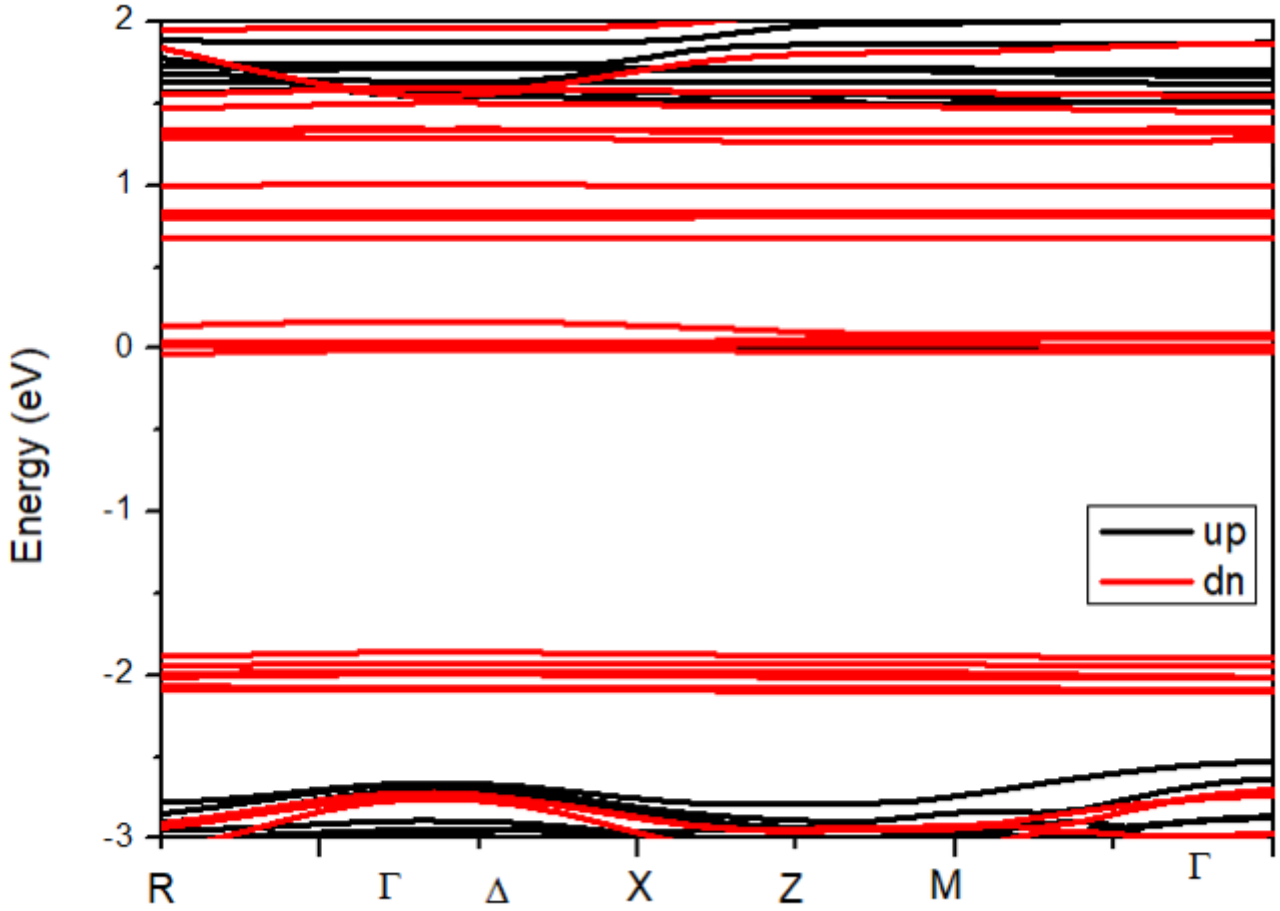

Figure 13

Band structure of (DyCe)Zr_2O_7.

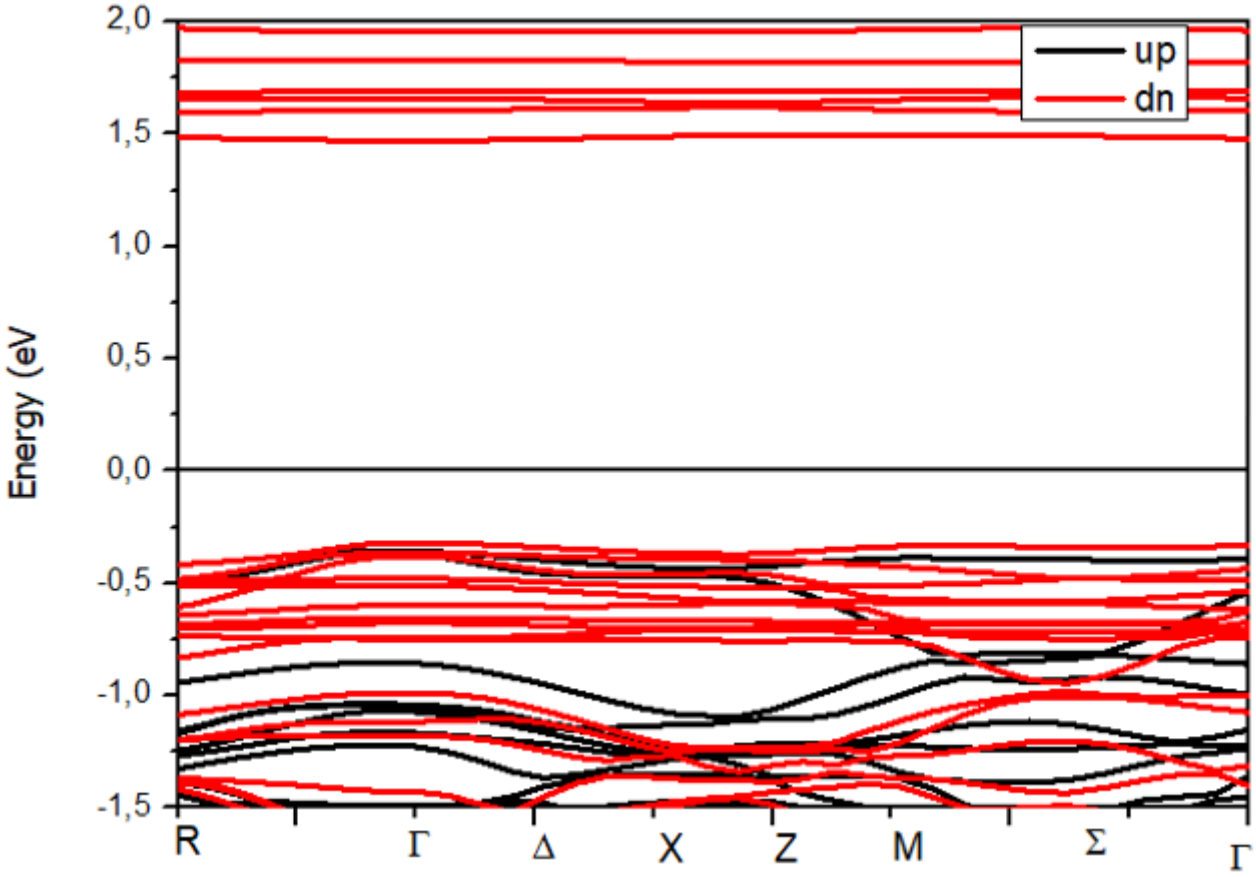

Figure 14

band structure of (DyCe)Zr_2O_7

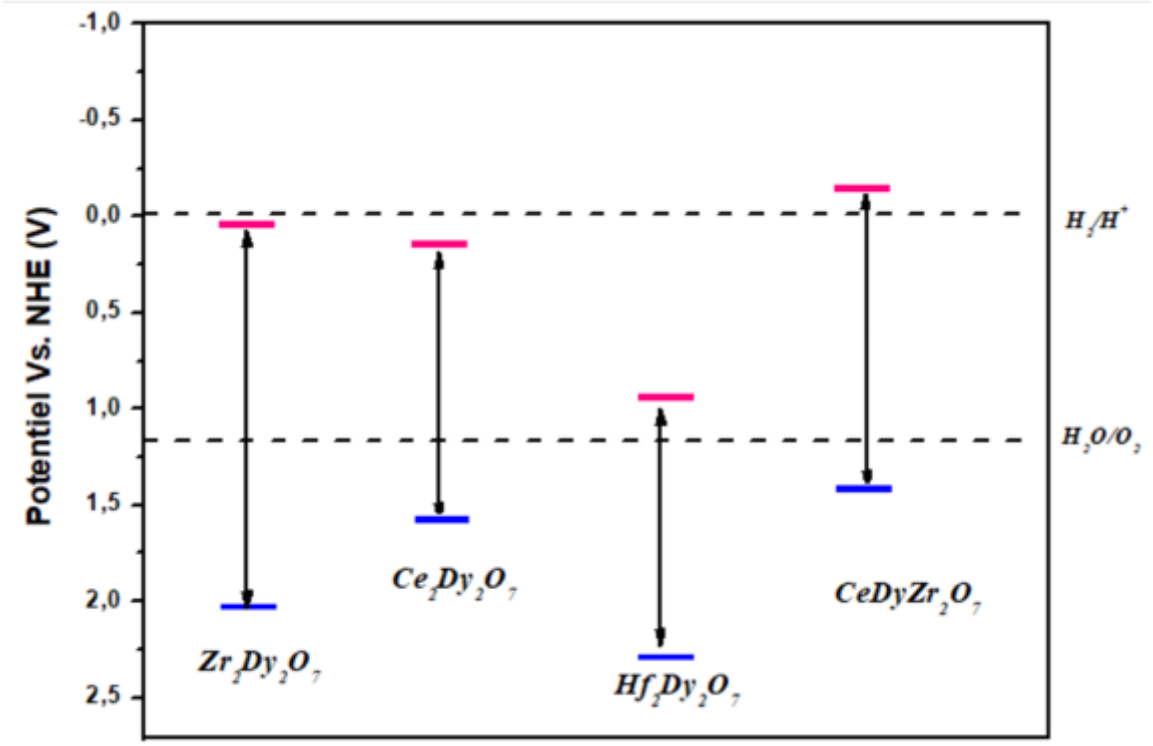

Figure 15

Electro-chemical potential (vs.NHE) of band edges of Dy(Ce/Hf/Zr)O_7